NEW SUBSTANCES, MATERIALS,
AND COATINGS

Effect of Pulsed Current Frequency on Morphology and Corrosion Behavior of Plasma Electrolytic Oxidation on Aluminum

Masoud Asgari[a], *, Alireza Sabour Rouhaghdam[a], and Ashkan Daneshmaslak[a]

[a] *Department of Materials Science, Faculty of Engineering, Tarbiat Modares University, Tehran, P.O. Box: 14115-143 Iran*
*e-mail: m_asgari23@yahoo.com

Abstract—Protective oxide coatings are developed on aluminum substrate through plasma electrolytic oxidation using a pulsed current and within the alkaline electrolyte. The morphology and corrosion resistance of the oxide layer established under a pulsed current condition have been previously carried out. Since the frequency is one of the main characteristics of the pulse current, the results were performed to investigate the effect of this factor. As the results specified, by increasing the pulse frequency, power of each pulse is individually reduced; therefore the required strength to break the dual capacitive layer on the sample surface is reduced. As a result, ignition is initiated at a higher voltage. The results show that with increasing time at a frequency of 10000 Hz and duty cycle of 25% the thickness was increased exponentially. It is also revealed that applying pulses with a higher frequency, can improve corrosion resistance significantly.

1. INTRODUCTION

Corrosion of aluminum has various types including: uniform, pitting, grain boundary, intergranular, exfoliation, tension, filiform, water line, crevice, cavitation, erosion, and microbial. Corroded areas are usually visible with naked eye [7, 31]. The most predominant type of corrosion is determined based on the balance of influencing factors such as metal's vulnerability, alloying elements, coating's characteristics and environment. However, there is not a specific type of corrosion for aluminum and its alloys [31]. In order to control corrosion rate of aluminum alloys, a few methods such as selection of appropriate alloy, system design, environment control, application of barriers and application of protective coatings have been utilized. Anodic oxide coatings may protect aluminum against corrosion, but they are not reliable for vulnerable alloys to corrosion [2, 14, 27]. Parameters which affect chemical electrolysis processes and plasma electrolytic oxidation (PEO) are almost identical. Fundamentally, properties of coatings developed by PEO method are affected by the nature of the substrate and alloying elements, type of power source, applied current density, anodic voltage limit, electrolyte composition and concentration, electrolyte temperature, anode and cathode distance from each other, electrolyte circulation and etc. [1, 6, 22, 25, 30]. A major parameter that must be controlled during the process is applied current density [3]. Based on the type of applied electric regime, power supplies can be divided into several groups. In this regard, the pulse direct current is among the best techniques in terms of the effect on the thickness and quality of the oxide layer [3, 8]. These power sources provide controllability over discharge duration and pulse shape. These advantages provide controllability over thermal conditions and therefore, the coating composition and structure are controllable [28, 37]. Using pulse sources, the possibility of forming a double layer of the discharge leads to an increase in creation of additional polarization on the electrode surface. Thereby, higher voltages (up to 1000 V) are required to achieve the desired current density. Overall, owing to the possibility of controlling time and discharge intensity through changing of duty cycles, oxidation process with pulse discharges has many advantages compared with DC or AC discharges [8, 21]. In the present study, we investigate effect of pulse current frequency on oxide coatings properties.

2. METHODS AND MATERIAL

Aluminum alloy 6082 extruded into rods with a diameter of 20 mm were used for coating. Surface of all samples were polished up to 2000 grit and degreased by immersing in an alcoholic solution. A 50×80 mm plate of grade 304 stainless steel was used as cathode. The composition of the electrolyte used in the experiments was 10 g/L of sodium aluminate ($NaAlO_2$) and 1.5 g/L of potassium hydroxide (KOH). The pH of solution was in the range of 12–12.5. Based on the surveys conducted before and after the process, it was
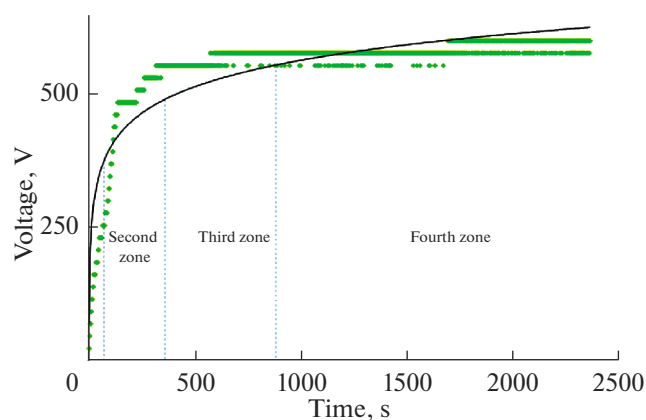
Fig. 1. Voltage changes with time curve during the PEO process.

Fig. 2. SEM micrographs of the sample surface morphology after about 90 seconds- before ignition. (a) 1000×; (b) 5000×; (c) 10 000×.

revealed that pH was almost constant even after coating treatment. Influence of frequency on coating micro-structure and corrosion resistance in solution of 3.5 wt % sodium chloride was studied. Potentiodynamic electrochemical polarization method was used for corrosion studies and the acquired results were analyzed by scanning electron microscopy (SEM). To study the role of low and high frequencies, three values of 100, 1000 and 10000 Hz were selected and investigated, respectively. Duty cycles of 25% and the coating times of 100 min were fixed.

3. RESULTS AND DISCUSSION

3.1. Voltage Variations against Time

Figure 1 represents voltage changes with time during PEO coating of the aluminum sample. The applied current density of 0.045 A/cm^2, the frequency of 10 000 Hz, and the duty cycle of 25% were adjusted. Almost four successive stages are differentiable by voltage and surface morphology variations over the process. Depending on the parameters of the process, the extent of these stages is varied.

The first stage is ascribed to conventional anodic oxidation. Through this stage, voltage soars linearly. During the first stage, oxygen bubbles form on the surface of the anode vigorously and no other significant changes are observed. At the end of first stage, very tiny fast-moving sparks sweep the surface [5, 13, 15, 29]. This stage lasts for about 90 seconds. Studying of electron microscope micrographs shown in Fig. 2, revealed that a very thin layer nucleates emerges on the surface and numerous tiny pores, with opening diameter of less than 100 nm, spread all over the surface. The non-uniform presence of the material surrounding the pores on the surface is also observed. The surface morphology in this stage is very similar to the one created by conventional anodizing method. It is important to note that at this stage the entire coating surface is not yet affected uniformly. In some areas,
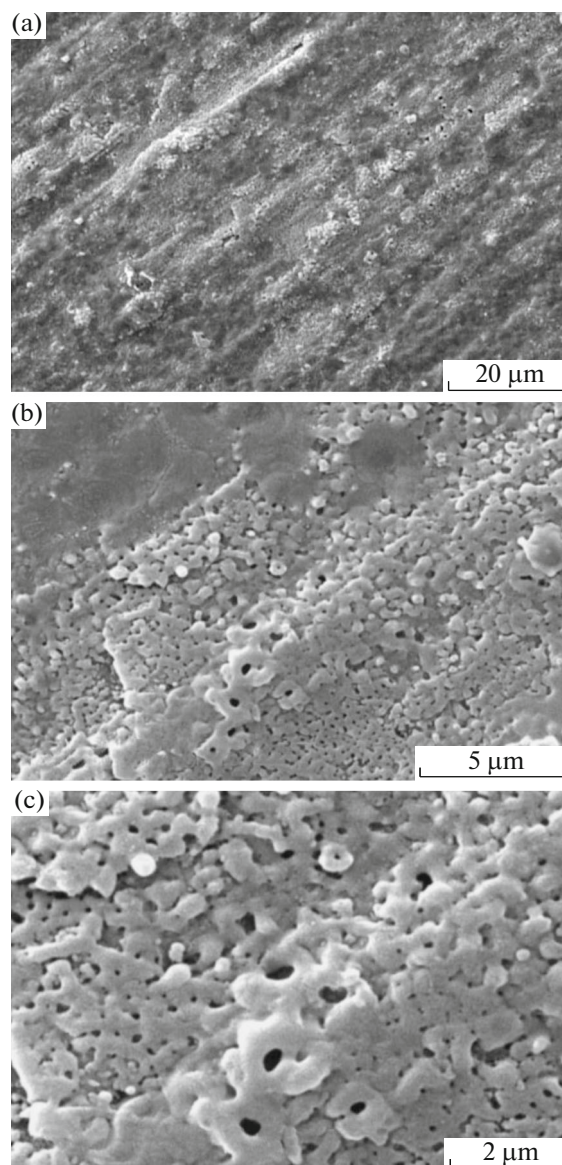
there are cooling craters representing the initiation of the second stage [11, 26].

In the second stage, rate of voltage changes declines and the curve follows a nonlinear trend. Since the beginning of this stage, micro arc discharges, associated with the phenomenon of luminescence, are visible by the naked eye. Gradually voltage rises and microarcs become slightly larger than those of the primary ones while their density reduces gradually. Moreover, their color changes slightly from glossy white to light yellow. At this stage, again the oxygen gas emissions occur strongly. The observations conducted on the sample surface indicate that the changes in color and surface roughness increased [30, 37]. Figure 3 illus-
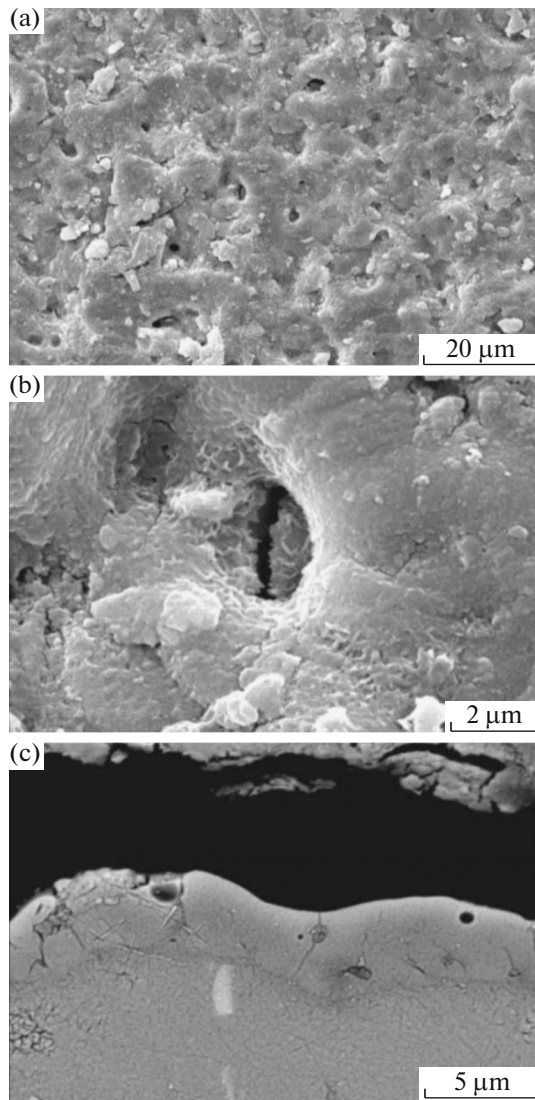
(a)

20 μm

(b)

2 μm

(c)

5 μm

Fig. 3. SEM micrographs of the surface morphology and cross section after about 5 min since the beginning of the process. (a) surface morphology−1000×; (b) surface morphology−7500×; (c) cross section−4000×.

20 μm

Fig. 4. SEM micrograph of the sample surface morphology after about 10 min from the beginning of the coating process magnified at 1000×.

trates SEM micrographs of the surface and free surface area of coating at this stage after about 5 min. As show in this figure, the sample surface is thoroughly coated. The coating has far fewer pores and porosities, while these pores are larger in size in comparison to the early stages. Frozen craters imply the presence of discharge channels on the surface of the coating. The opening diameters of these volcanoes are about 4 μm which is indicative of formation of micro sparks.

Higher magnification micrographs of the coating surface, Fig. 3b, present a specific microstructure, which is possibly indicative of rapid solidification of the molten material. In Fig. 3c, cross section of the developed coating is shown. The thickness of this coating is about 4 μm. By increasing the voltage, the
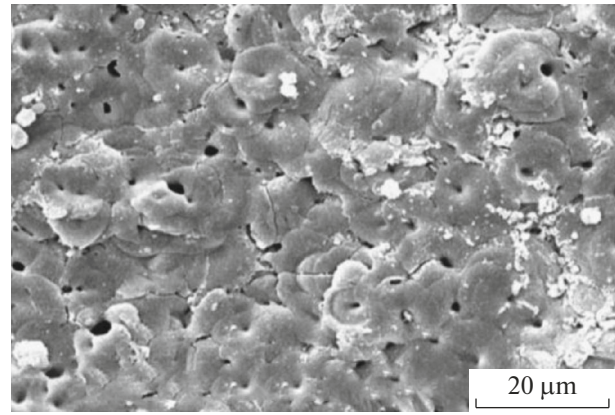
process enters to the third stage, where the curve has almost a linear trend. Increasing rate of voltage and monitoring revealed that the density of micro sparks is reduced and the tiny sparks join and form larger sparks. In general, sparks are more sluggish than the initial state and move slowly over the surface. The color of the sparks tends to change towards deep yellow. Besides, the intensity of the oxygen emission reduces due to reduction of ignition rate. SEM micrograph of the free surface after about 10 min is shown in Fig. 4. The area of each microdischarge and pore diameter is enlarged compared to second stage and the surface becomes rougher. Studying micrographs revealed that samples' surface are completely covered with craters that are enlarged after this phase [16, 32].

After this stage, by a further increase in voltage, the process enters to the fourth stage (Fig. 1). In this step, voltage changes with time linearly again. No significant change is noticed in the curve slope during the coating period. Observations show a sharp drop in the number of sparks while they become larger. The color of the sparks becomes notable and varies from pale orange to deep orange. With the increase coating duration at this stage, a handful of sparks appear which reaches zero in some states. The process is completed at this stage and the coating damage occurs. Furthermore, gas emissions from the coating surface also decline sharply, as they appear only at spark ignition sites. Figures 4 and 5 illustrate the SEM micrograph of the surface and surface area of the sample after about 60 min. As shown, craters continue to increase and their density decreases. In other words, the number of sparks and their dimensions become less and larger, respectively. Due to the very high number of melting and re-freezing oxide coating up to this time, most craters are turned off and blocked with the neighboring volcanos [18].

As the four-stage division is taken into account for the PEO process in most references, the voltage varia-
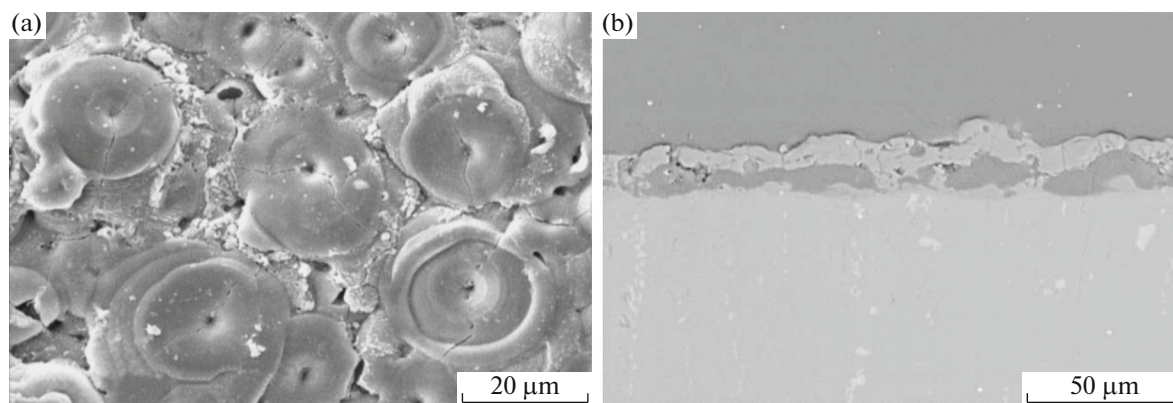
Fig. 5. SEM micrographs of the surface morphology and specimen surface area for about 60 min after the start of the process. (a) 1000×; (b) 500×.

tion curves with time are examined on this basis [18, 32, 33]. Dehnavi et al. [9, 10, 12, 24] outlined the steps of this process in their work.

3.2. The Effect of Applied Current Frequency on Ignition Voltage and Sparks Distribution

In this research, ignition voltage on the given sample was considered as a reference to compare and evaluate the quality of the process's implementations. In Fig. 6, the results obtained during tests are expressed as a graph. With increasing frequency, ignition voltage also increases. Based on its definition (the number of pulses which are established in one second), frequency (ν) is the reverse of period (T). The higher the frequency of the applied current, the more the number of pulses per unit time and pulses become narrower. By placing the aluminum sample in a corrosive alkaline solution (pH ~ 12), a double layer, known as capacitive layer, is created at the interface of aluminum surface and electrolyte. Additional polarization is attributed to the presence of this layer on the surface. To perform ignition on the sample surface, current must be trans-
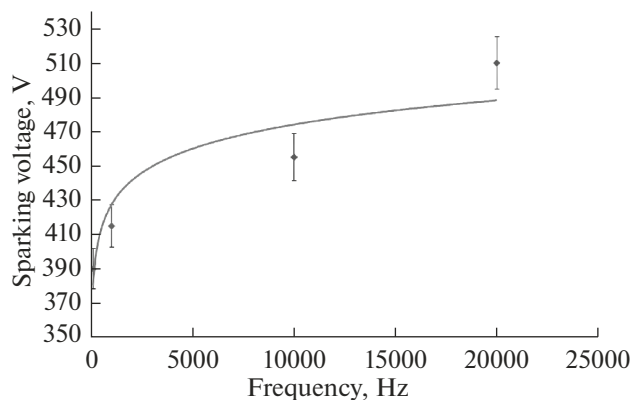
ferred from the resistance of this capacitor to surface. In fact, the pulse must have enough strength to break this layer. The amount of work required to pass the charge from this capacitor layer is equal to $V \times I \times \tau$. In all tests, the current density is kept constant, so the current amount is the same for all frequencies. Increasing frequency, τ, means that the pulse-on duration decreases, correspondingly the value of ignition potential V should be increased.

Figure 7 shows that when the frequency increases, the time interval in which a pulse-on occurs is decreased. By reducing the time of a pulse-on, ignition time is shortened. Observations conducted during tests confirm our suggestion where at the beginning of sparking at higher frequency sparks are finer and as a result their density increases and sparks cover the entire surface uniformly. On the other hand, after the lapse of time since the beginning of the process although the sparks get larger, the micro sparks are still observed and the duration of staying-on craters is significantly reduced [24, 28, 35]. Similarly Arunnellaiappan et al. [4] reported that in the first sparks the number of micro sparks is greater and they become larger and less frequent by the passage of time. They reported that the voltage initially rises with time and then, as the thickness reaches the critical value, it acts as an intermediate resistance and subsequently failure occurs in layers and ignition starts. In this regard, Yao et al. [26] reported the same results.

3.3. The Effect of Applied Current Frequency on the Surface Morphology and Oxide Layer Thickness

To make clear the differences, results of samples coating with 100 and 10 000 Hz frequency was reported in this section. Figures 8a, 8b indicates that when frequency rises, the density of craters increases and subsequently these openings become smaller [15, 23]. In support of this, in Fig. 8c for frequency of 100 Hz the diameter of crater opening was measured approximately 51 μm, while in Fig. 8d at frequency of 10 000 Hz,
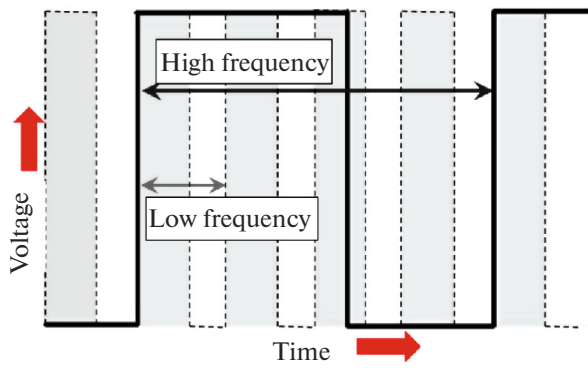

Fig. 6. Ignition voltage changes relative to the applied current frequency.

Fig. 7. The effect of pulse frequency increase on its form. Dotted lines show the pulse with higher frequency.

surements conducted on the micrographs indicate that at the frequency of 100 Hz, the extent of cracks becomes greater while their openings become wider. In magnification of 500 times and the rectangular dimensions of $130 \times 190 \ \mu m^2$, in Fig. 9a, the total length of the cracks was measured approximately 413 μm; but as shown in Fig. 9b, the monitored cracks had a more limited extent with more closed openings. The total length corresponding to these cracks are about 190 μm.

Micrographs of free surface of these two samples are presented in Fig. 10. The results of previous works indicate that in both cases the PEO coating continuously covers the sample surface. The measured coating thickness was about 50 μm for Fig. 10a and 77 μm for Figure 10b. Based on the processing duration, nucleation rate can be estimated which is 0.5 μm/min and 0.77 μm/min for 100 and 10 000 Hz, respectively. The difference in coating nucleation rate can be explained with the fact that at the low frequency the number of sparks per unit of time is less but they are more powerful. Thus, they form larger and deeper tunnels in the coating and gives rise to exiting lava in larger volumes through the tunnels. However, it should be emphasized that such a phenomenon occurs rarely. Furthermore, these coatings possess more defects in their structure [17].
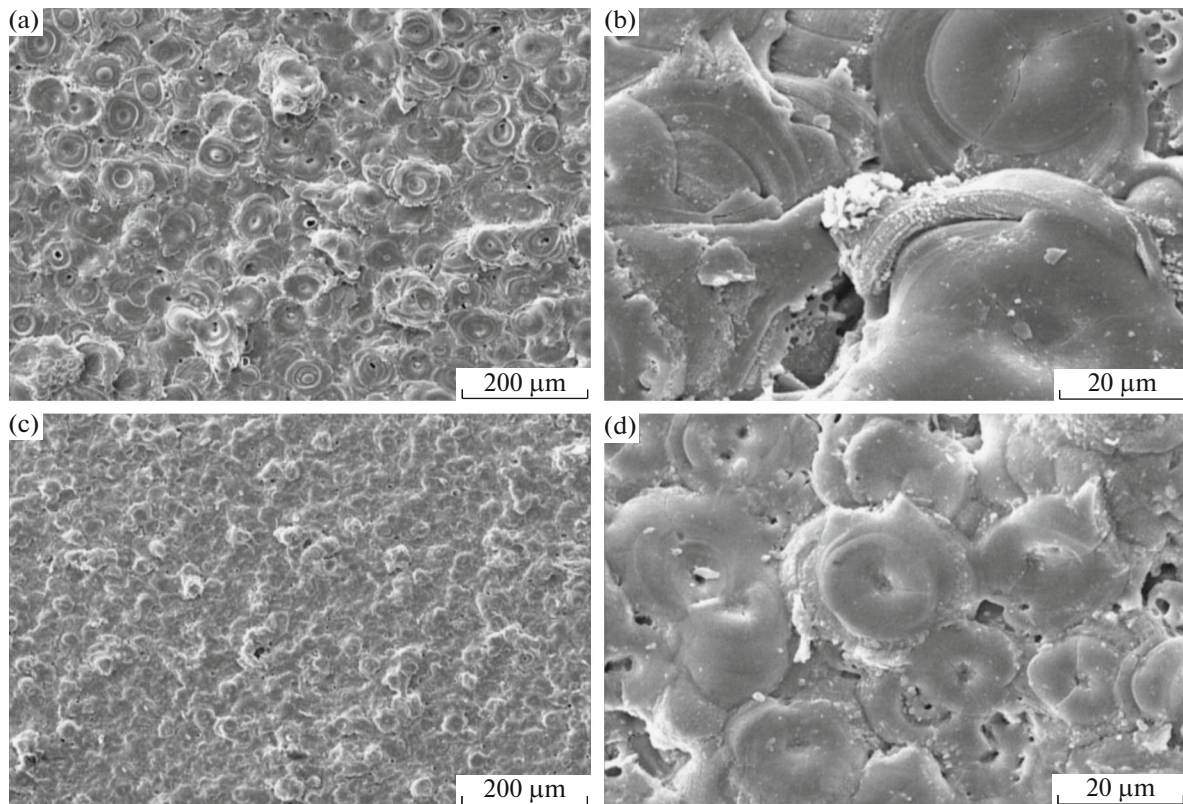
diameter is about 20 μm. For frequency of 1000 Hz the diameter of crater opening was measured approximately 27 μm. Observations conducted during the test suggest that when PEO process is carried out at higher frequencies, the density of micro sparks is greater compared to lower frequencies. Observations were confirmed with surface micrographs of the samples. The presence of cracks on the surface of two samples is compared in terms of size and length in Fig. 9. Mea-

Fig. 8. SEM micrograph of the coating surface (a) and (b) frequency of 100 Hz; (c and d) frequency of 10 000 Hz. (a) and (c) 100×, (b and d) 1000×.
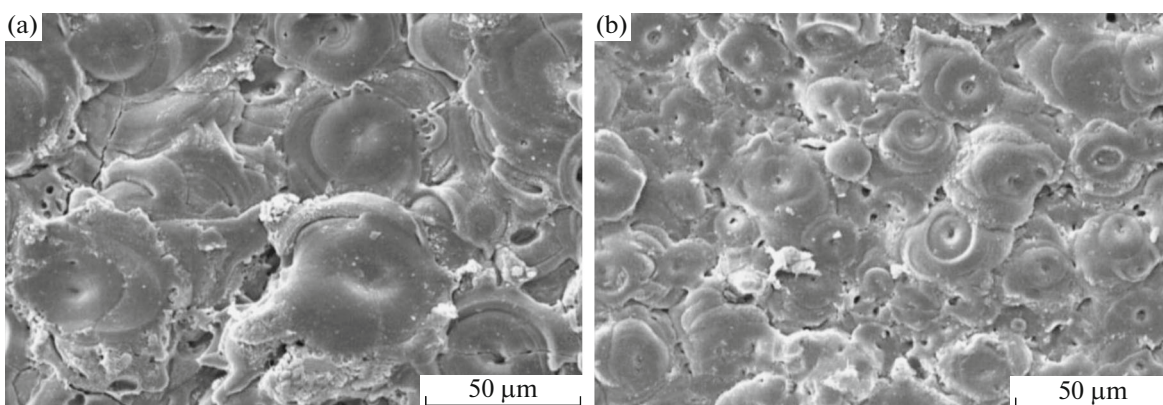
Fig. 9. Comparison of cracks area in the coating of PEO created in frequency (a) 100; (b) 10000 Hz. Micrographs scale 500×.
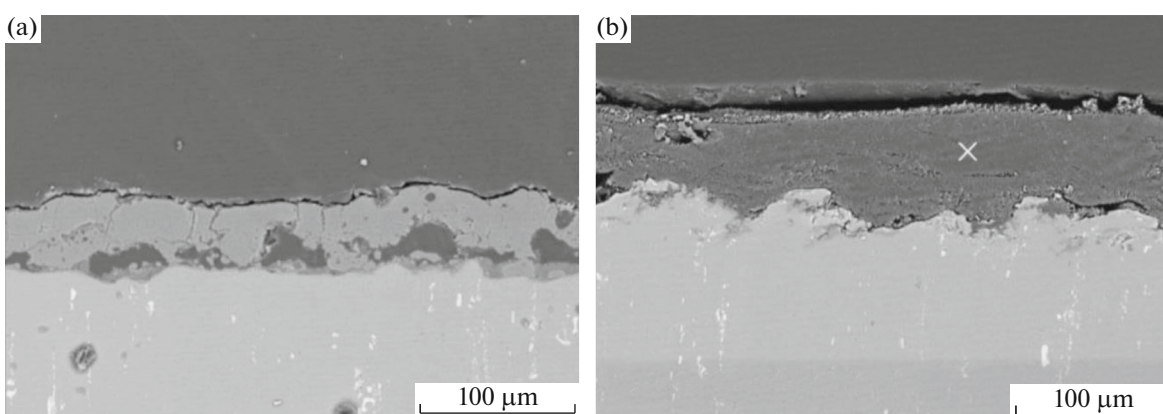

Fig. 10. Comparison of the coating thickness obtained in frequency (a) 100; (b) 10 000 Hz.

When the frequency is high, the number of sparks per unit time increases, but their power diminishes. Therefore, sparks melt lesser volume of material that is conveyed out in smaller tunnels. Nevertheless, because their number is much higher in unit volume, the coating nucleation rate will be consequently higher in this mode. Besides, due to the high density of the sparks, the structure possesses a greater density and fewer defects [34, 38]. Figure 11 demonstrates the distribution of electric discharge tunnels in the coating section for both frequencies. In Fig. 10b, the large scale tunnels are not demonstrated and the structure has a very high density.

Lv et al. [20] studied magnesium coating by PEO method with pulsed current and reported the similar results. They reported that at low frequencies the diameter of the pores was larger than that of high frequencies. They also confirmed that by increasing the coating time cracks enlarge in the sample coated with a lower frequency, leading to more damage in the coating. Their results showed lower frequencies lead to rougher surfaces.

3.4. Phase Composition

As shown in Fig. 10, X-ray diffraction (XRD) analysis was performed on the surface of samples. The peaks shown in this figure demonstrate that aluminum is the main phase also γ-Al_2O_3 phase and a small percentage of the α-Al_2O_3 phase were detected.

The most important point about these results is that aluminum is the main phase, whereas given the current operating conditions and theories expressed, the sample surface should be coated with oxide layers. This behavior can be attributed porous nature of the coating which results in diffusing of emitted rays in to the depth of the aluminum substrate. This argument is also mentioned in some other references. In addition, and most likely, presence of aluminum substrate within the coating may be due to the poor quality of the coating formed, implying absence of ideal conditions for coating development. This fact is due to the lack of access to coating synthesis technology.

In addition to presence of some discharge channels, surface pores, and heat cracks created the coating somewhat is subject to a corrosive solution in contact with its surface. In addition, the existence of some
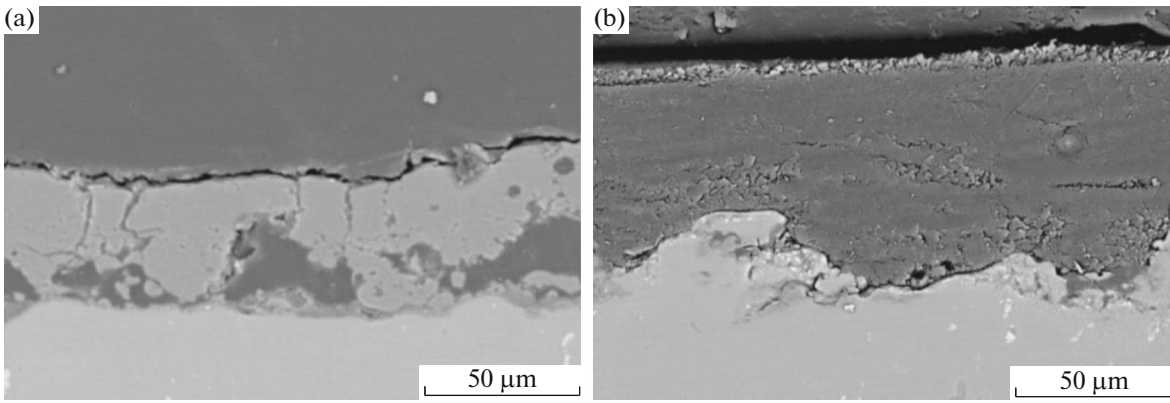
Fig. 11. Distribution of discharge tunnels in the coating thickness in frequency (a) 100, (b) 10000 Hz.

impurities and other compounds, which are poor, compared with corrosion, a severe corrosion and large pores are formed in these areas. As mentioned above, the XRD results demonstrate the presence of aluminum substrate in the coating. Thus, these areas would have a poor corrosion resistance compared to the ones formed on alumina. Arunnellaiappan et al. [4] reported that the coating peaks are generally indexed with gamma alumina phase in the phase composition and aluminum that is probably related to the substrate. After these two peaks, the peak related to alpha alumina is apparent [19, 23].
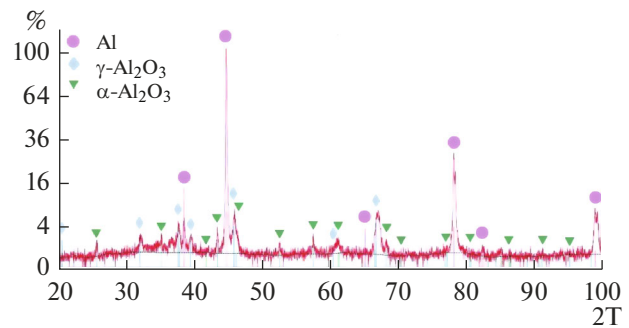

Fig. 12. XRD image of the surface coating.

3.5. The Effect of Applied Current Frequency on PEO Coatings Corrosion Resistance

Figure 8 presents potentiodynamic polarization of coated samples. Both of coated samples show about 3 orders of magnitudes reduction in corrosion current density compared to bare metal. Corrosion current density of the sample coated at frequency of 10000 Hz is lower than the sample coated at 100 Hz. However, the difference in corrosion current density at low voltages is lesser compared to higher voltages. This situation starts from approximately 100 mV above the open circuit potential. At high frequencies the corrosion resistance of the developed layer is better than it generated from applying current at the low frequency [28]. As a proof of this claim, the thickness of the coating developed in both modes, morphology, distribution

pattern, and the extent of surface cracks were investigated. As shown in Fig. 4 and as described in section 2–3, at low frequencies the density of sparks is lower and therefore one of discharge channels is lower, as well. Discharge channels created at high-frequency currents have a smaller diameter and it seems that the craters in this case are blocked in most areas of the surface [4]. In addition, Figs. 5a, 5b indicate that surface cracks have a smaller width when the current frequency is higher. By careful examining of Fig. 6, the coating thickness was measured for both modes.

The greater coating density at higher current frequencies may be the other reason for the higher corrosion resistance. By comparing Figs. 7a, 7b, it was also observed that the oxide layer generated at a higher fre-

Table 1. The results of potentiodynamic polarization at different applied current frequencies

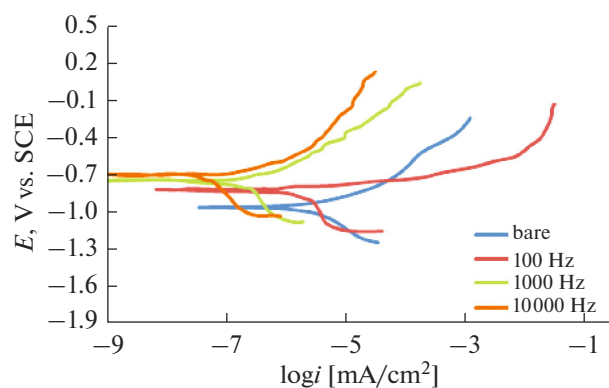| Sample	Frequency, Hz	E_{corr}, mV	I_{corr}, $\times 10^{-7}$ A/cm^2	β_a, $\times 10^{-1}$ V/decade	β_c, $\times 10^{-1}$ V/decade
	Bare	−923.7	45.923	113.473	65.727
00	100	−831.1	31.623	0.8806	7.118
02	1000	−758.9	2.723	3.341	9.246
11	10000	−710.6	1.076	3.437	6.576

Fig. 13. Potentiodynamic polarization diagram at different pulsed current frequencies for the coated specimens by PEO method.

quency has a more density and less distribution of pores. In this regard, presence of cracks in the coating surface area could be another reason for the higher corrosion resistance [17]. These evidences justify the difference in corrosion resistance in both modes, but generally porous structure, defects and unwanted compounds in the coating composition in both modes would lead to the failure of polarization curves and reduce the corrosion resistance at higher potentials [10, 11].

Considering the corrosion current density, it can be generally stated that in all samples application of PEO coating reduces corrosion current and thus increases the corrosion resistance of the coating. However, it must be noted that the current density in corrosion potential poses only a relative factor and its reduction can never be a mere reason for increase of corrosion resistance. In this study, the effect of anodic branch in PEO coating on corrosion resistance was investigated. Arunnellaiappan et al. [4], who examined the effect of frequency and duty current cycle on aluminum alloys, reported that the frequency and duty cycle have significant effects on morphology, composition thickness, and corrosion resistance.

4. CONCLUSION

1. The increase in pulse frequency resulted in reduction of the power of each pulse; thus, the required strength to break dual capacitive layer on the surface is lowered. As a result, ignition is initiated at a higher voltage.

2. By increasing the coating duration at frequency of 10000 HZ and duty cycle of 25%, the thickness increased exponentially.

3. With increasing pulse frequency, sparks' density is increased and oxygen evolution occurs vigorously. Ignition quality is improved and the surface becomes covered with micro pores. Surface defects such as micro cracks are reduced and the coating thickness increases as well.

4. The developed layer is resistant to corrosion, but pitting was observed in defective areas. The observed defects include open-mouth pores and cracks on the coating surface.

5. With increasing coating thickness, followed by densification of the intermediate layers, the corrosion resistance of such coatings increased. Increasing of current frequency improves corrosion resistance.

REFERENCES

1. Aliofkhazraei, M. and Rouhaghdam, A.S., *Electrochem. Commun.,* 2012, vol. 20, pp. 88−91.

2. Aliofkhazraei, M. and Rouhaghdam, A.S., *Surf. Coat. Technol.,* 2011, vol. 205, pp. S57−S62.

3. Aliofkhazraei, M., Rouhaghdam, A.S., and Gupta, P., *Crit. Rev. Solid State Mater. Sci.,* 2011, vol. 36, no. 3, pp. 174−190.

4. Arunnellaiappan, T., Kishore Babu, N., Rama Krishna, L., and Rameshbabu, N., *Surf. Coat. Technol.,* 2015, vol. 280, pp. 136−147.

5. Asgari, M., Aliofkhazraei, M., Darband, G.B., and Rouhaghdam, A.S., *Surf. Coat. Technol.,* 2017, vol. 309, pp. 124−135.

6. Barati Darband, G., Aliofkhazraei, M., Hamghalam, P., and Valizade, N., *J. Magnesium Alloys,* 2017, vol. 5, no. 1, pp. 74−132.

7. Barik, R.C., Wharton, J.A., Wood, R.J.K., Stokes, K.R., and Jones, R.L., *Surf. Coat. Technol.,* 2005, vol. 199, nos. 2−3, special issue, pp. 158−167.

8. Curran, J. and Clyne, T., *Surf. Coat. Technol.,* 2005, vol. 199, no. 2, pp. 168−176.

9. Dehnavi, V., Liu, X.Y., Luan, B.L., Shoesmith, D.W., and Rohani, S., *Surf. Coat. Technol.,* 2014, vol. 251, pp. 106−114.

10. Dehnavi, V., Luan, B., Liu, X.Y., Shoesmith, D.W., and Rohani, S., *Proc. Materials Science and Technology Conference and Exhibition MS&T'13,* Montreal, 2013.

11. Dehnavi, V., Luan, B.L., Liu, X.Y., Shoesmith, D.W., and Rohani, S., *Surf. Coat. Technol.,* 2015, vol. 269, no. 1, pp. 91−99.

12. Dehnavi, V., Shoesmith, D.W., Luan, B.L., Yari, M., Liu, X.Y., and Rohani, S., *Mater. Chem. Phys.,* 2015, vol. 161, pp. 49−58.

13. Dehnavi, V., Shoesmith, D.W., Luan, B.L., Yari, M., Liu, X.Y., and Rohani, S., *Mater. Chem. Phys.,* 2015, vol. 161, pp. 49−58.

14. Gheytani, M., Aliofkhazraei, M., Bagheri, H.R., Masiha, H.R., and Rouhaghdam, A.S., *J. Alloys Compd.,* 2015, vol. 649, pp. 666−673.

15. Gheytani, M., Bagheri, H.R., Masiha, H.R., Aliofkhazraei, M., Sabour Rouhaghdam, A., and Shahrabi, T., *Surf. Eng.,* 2014, vol. 30, no. 4, pp. 244−255.

16. Golabadi, M., Aliofkhazraei, M., Toorani, M., and Sabour Rouhaghdam, A., *J. Ind. Eng. Chem.,* 2017, vol. 47, p. 154−168.

17. Gu, Y., Ning, C., Yu, Z., Li, H., Xiong, W., and Chen, L., *Xiyou Jinshu Cailiao Yu Gongcheng/Rare Met. Mater. Eng.,* 2014, vol. 43, no. 10, pp. 2463−2468.

18. Guan, Y., Xia, Y., and Li, G., *Surf. Coat. Technol.,* 2008, vol. 202, no. 19, pp. 4602−4612.

19. Guangliang, Y., Xianyi, L., Yizhen, B., Haifeng, C., and Zengsun, J., *J. Alloys Compd.,* 2002, vol. 345, no. 1, pp. 196−200.

20. Lv, G.H., Chen, H., Gu, W.C., Li, L., Niu, E.W., Zhang, X.H., and Yang, S.Z., *J. Mater. Process. Technol.,* 2008, vol. 208, nos. 1−3, pp. 9−13.

21. Mann, R., Hansal, W.E.G., and Hansal, S., *Trans. Inst. Met. Finish.,* 2014, vol. 92, no. 6, pp. 297−304.

22. Masiha, H.R., Bagheri, H.R., Gheytani, M., Aliofkhazraei, M., Sabour Rouhaghdam, A., and Shahrabi, T., *Bull. Mater. Sci.,* 2015, vol. 38, no. 4, pp. 935−943.

23. Nie, X., Meletis, E., Jiang, J., Leyland, A., Yerokhin, A., and Matthews, A., *Surf. Coat. Technol.,* 2002, vol. 149, no. 2, pp. 245−251.

24. Parfenov, E.V., Yerokhin, A.L., and Matthews, A., *Surf. Coat. Technol.,* 2007, vol. 201, no. 21, special issue, pp. 8661−8670.

25. Seyfoori, A., Mirdamadi, S., Seyedraoufi, Z.S., Khavandi, A., and Aliofkhazraei, M., *Mater. Chem. Phys.,* 2013, vol. 142, no. 1, pp. 87−94.

26. Sharifi, H., Aliofkhazraei, M., Darband, G.B., and Rouhaghdam, A.S., *Surf. Coat. Technol.,* 2016, vol. 304, pp. 438−449.

27. Sharifi, H., Aliofkhazraei, M., Darband, G.B., and Rouhaghdam, A.S., *Tribol. Int.,* 2016, vol. 102, pp. 463−471.

28. Song, X., Lu, J., Yin, X., Jiang, J., and Wang, J., *J. Magnesium Alloys,* 2013, vol. 1, no. 4, pp. 318−322.

29. Toorani, M., Aliofkhazraei, M., Golabadi, M., and Rouhaghdam, A.S., *J. Alloys Compd.,* 2017, vol. 719, pp. 242−255.

30. Toorani, M., Aliofkhazraei, M., Naderi, R., Golabadi, M., and Sabour Rouhaghdam, A., *J. Ind. Eng. Chem.,* 2017, vol. 53, pp. 213−227.

31. Vargel, C., *Corrosion of Aluminium,* Elsevier, 2004.

32. Xu, F., Xia, Y., and Li, G., *Appl. Surf. Sci.,* 2009, vol. 255, no. 23, pp. 9531−9538.

33. Xu, J., Liu, F., Luo, J., and Zhao, L., *J. Mater. Sci. Technol.,* 2013, vol. 29, no. 1, pp. 22−28.

34. Yao, J., Chen, M., Ma, Y., Zheng, H., and Xu, W., *Tezhong Zhuzao Ji Youse Hejin/ Spec. Cast. Nonferrous Alloys,* 2010, vol. 30, no. 6, pp. 570−572.

35. Yao, Z., Cui, R., Jiang, Z., and Wang, F., *Appl. Surf. Sci.,* 2007, vol. 253, no. 16, pp. 6778−6783.

36. Yerokhin, A., Nie, X., Leyland, A., Matthews, A., and Dowey, S., *Surf. Coat. Technol.,* 1999, vol. 122, no. 2, pp. 73−93.

37. Yerokhin, A., Snizhko, L., Gurevina, N., Leyland, A., Pilkington, A., and Matthews, A., *J. Phys. D: Appl. Phys.,* 2003, vol. 36, no. 17, p. 2110.

38. Yerokhin, A., Voevodin, A., Lyubimov, V., Zabinski, J., and Donley, M., *Surf. Coat. Technol.,* 1998, vol. 110, no. 3, pp. 140−146.